*Journal of Organometallic Chemistry*, 437 (1992) 211-225
Elsevier Sequoia S.A., Lausanne
JOM 22785

# Catalytic de-ligation of bis(arene)iron dications upon electro-reduction *

Z.J. Karpinski [1] and J.K. Kochi
*Chemistry Department, University of Houston, Houston, TX 77204-5641 (USA)*

(Received February 7, 1992)

## Abstract

Bis(arene)iron(II) dications ($Ar_2Fe^{2+}$) suffer the facile loss of aromatic ligands with Ar = hexamethylbenzene (HMB), durene (DUR), and mesitylene (MES), when acetonitrile solutions are exposed to reducing conditions. Electrocatalysis of the arene deligation is established during the controlled cathodic reduction of $Ar_2Fe^{2+}$ by catalytic turnover numbers of 20, 75 and 150 for Ar = HMB, DUR and MES. Cyclic voltammetry of $Ar_2Fe^{2+}$ reveals a pair of waves $P_1$ and $P_2$ for the 1-electron couples $Ar_2Fe^{2+/+}$ and $Ar_2Fe^{+/0}$, respectively, the chemical reversibility of which depends on the donor strength of the arene ligand in order: Ar = HMB > DUR > MES. The detailed examination of the dependence of the peak current ratio $i_p^a/i_p^c$ for $P_1$ with the CV sweep rate points to the monocation $Ar_2Fe^+$ as the labile intermediate leading to arene deligation. The mechanistic discussion for electrocatalysis centers around the further oxidation of the metastable $Fe(NCCH_3)_6^+$ at the electrode (ECE) or by $Ar_2Fe^{2+}$ (HOMO). First-order rate constants for the deligation of the neutral $Ar_2Fe^0$ are also evaluated from the CV analysis of $P_2$.

## Introduction

Bis(arene)iron dications $(Ar)_2Fe^{2+}$ are excellent organometallic acceptors by virtue of their electron-deficient centers on iron [1-3]. In this capacity, they readily interact with various electron donors (D) to form an interesting series of 1:1 electron donor-acceptor (EDA) complexes [4], *i.e.*:

$$Ar_2Fe^{2+} + D \rightleftharpoons [Ar_2Fe^{2+}, D] \qquad (1)$$

When the donors are electron-rich organometals such as D = ferrocene [5], the formation of the EDA complexes is accompanied by the appearance of a new

---

Correspondence to: Dr. J.K. Kochi.

* Dedicated to Professor Alwyn G. Davies in recognition of his distinguished contributions to organometallic chemistry.

[1] Permanent address: Department of Chemistry, University of Warsaw, Pasteura 1, PL-02093 Warsaw, Poland.

(visible) absorption band that is associated with an intermolecular charge-transfer transition of the type originally identified by Mulliken [6,7]. Most notably, we found that the deliberate irradiation of the charge-transfer bands with monochromatic light led to the efficient deligation of the bis(arene)iron(II) complexes [4], *i.e.*:

$$Ar_2Fe^{2+} \xrightarrow[CH_3CN]{[D]} 2Ar + Fe^{2+} \tag{2}$$

Furthermore, the same process occurred spontaneously in the dark when $Ar_2Fe^{2+}$ was merely exposed to other very electron-rich donors. In both cases, the facile deligation of arene ligands was ascribed to the metastable bis(arene)iron(I) monocation [8] ($Ar_2Fe^+$) formed as the transient intermediate in the photo-induced ($h\nu_{CT}$) or thermally allowed ($\Delta$) oxidation–reduction within the EDA complex, *i.e.*:

$$[Ar_2Fe^{2+}, D] \xrightarrow[\text{or } \Delta]{h\nu_{CT}} [Ar_2Fe^+, D^+] \tag{3}$$

$$[Ar_2Fe^+, D^+] \xrightarrow[\text{fast}]{} 2Ar + Fe^{2+} + D \tag{4}$$

Scheme 1.

In this report, the direct electrochemical reduction of the bis(arene)iron(II) complex is shown to be an unambiguous method for accessing the metastable (19-electron) cation. Most importantly, we utilize electrochemical methodology to provide an independent examination of the transient chemical behavior of $Ar_2Fe^+$ in the absence of the electron donor (eq. 4).

## Results

The bis(arene)iron(II) complexes with arene = hexamethylbenzene (HMB), durene (DUR) and mesitylene (MES) offer a graded series of electron acceptors owing to their increasingly positive reduction potentials of $E^\circ_{red} = -0.68$, $-0.58$ and $-0.49$ V *vs.* ferrocene, respectively. The overall energy span of $\sim 5$ kcal $mol^{-1}$ between $(HMB)_2Fe^{2+}$ and $(MES)_2Fe^{2+}$ was sufficient to readily delineate the pertinent kinetic differences of $Ar_2Fe^+$ resulting from the change in arene ligands in the following manner.

### *I. Cyclic voltammetry of bis(arene)iron(II) dications. Estimated lifetimes of the 19- and 20-electron intermediates*

Orange solutions of the bis(arene)iron(II) hexafluorophosphate salts: $(HMB)_2Fe^{2+}(PF_6^-)_2$, $(DUR)_2Fe^{2+}(PF_6^-)_2$, and $(MES)_2Fe^{2+}(PF_6^-)_2$, in acetonitrile containing tetra-n-butylammonium hexafluorophosphate (0.1 *M* TBAH) as the supporting electrolyte were stable at a platinum electrode for more than 5 h, when carefully protected from light.

The initial negative-scan cyclic voltammogram (CV) of the hexamethylbenzene complex $(HMB)_2Fe^{2+}$ revealed a pair of one-electron cathodic peaks $P_1$ and $P_2$ (Fig. 1A) to reflect the successive reduction of the dication to the 19-electron monocation and then to the 20-electron neutral complex [8], *i.e.*:

$$(HMB)_2Fe^{2+} \overset{P_1}{\rightleftharpoons} (HMB)_2Fe^+ \overset{P_2}{\rightleftharpoons} (HMB)_2Fe^0 \tag{5}$$

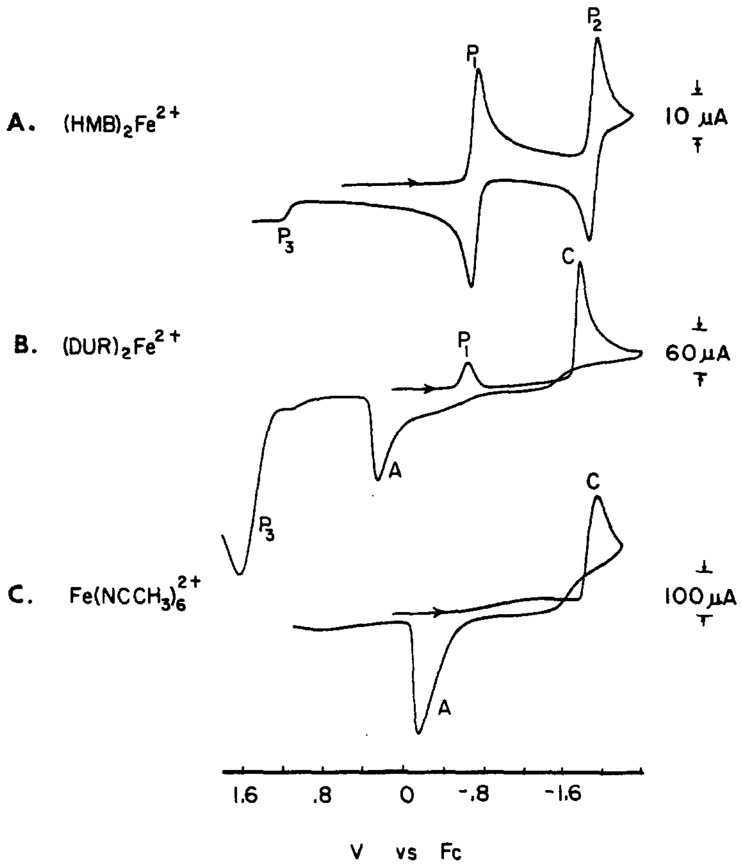

Fig. 1. Initial negative-scan cyclic voltammograms of (A) 1.9 m*M* $(HMB)_2Fe^{2+}$, (B) 3.7 m*M* $(DUR)_2Fe^{2+}$, and (C) 5 m*M* $Fe(NCCH_3)_6^{2+}$ in acetonitrile at $v = 0.5$ V $s^{-1}$.

At potential scan rates faster than 2 V $s^{-1}$, both redox couples exhibited chemical reversibility, as shown by the ratios of anodic/cathodic peak currents, $i_p^a/i_p^c$, that were close to unity. The observed shapes of the current–potential curves indicated fast heterogeneous electron transfer rates, the cyclic voltammograms being close to those of diffusion-controlled electrode reactions. Thus, the peak currents were proportional to the square root of the CV scan rate ($v^{1/2}$) and the peak potential difference, increased from 75 mV at $v = 2$ V $s^{-1}$ to 150 mV at 100 V $s^{-1}$ in a manner reminiscent of that observed for the reversible oxidation of ferrocene under the same experimental conditions [9,10]. Moreover, the formal potentials of $(HMB)_2Fe^{2+}/(HMB)_2Fe^{+}$ and $(HMB)_2Fe^{+}/(HMB)_2Fe^{0}$, calculated as $(E_p^c - E_p^a)/2$ [11,12], were independent of the potential sweep rate (within ±10 mV) as $v$ was varied from 0.5 to 200 V $s^{-1}$ (Table 1). Most notably, the peak current ratio $i_p^a/i_p^c$ gradually decreased at scan rates slower than $v = 1$ V $s^{-1}$, and it was simultaneously accompanied by the growth of a new anodic peak $P_3$ due to free (uncomplexed) hexamethylbenzene. These changes indicated some instability of $(HMB)_2Fe^{+}$ and $(HMB)_2Fe^{0}$ in acetonitrile solution, which was evident only during the slowest CV experiments.

Table 1

Deligation rates of bis(arene)iron(I) and bis(arene)iron(0) from CV peak current ratios [a]

| $Ar_2Fe^{+/0}$ | (m*M*) | $v$ ($V\ s^{-1}$) | $E^0$ (V) [b] | $i_p^a / i_p^c$ | $k_T$ [c] | $k_1'$ ($s^{-1}$) [d] | $k_2'$ ($s^{-1}$) [d] |
|---|---|---|---|---|---|---|---|
| $(HMB)_2Fe^+$ | (4.8) | 1.6 | −0.681 | 0.98 | 0.027 | 0.107 | |
| | | 0.8 | −0.681 | 0.96 | 0.05 | 0.10 | |
| | | 0.4 | −0.678 | 0.91 | 0.10 | 0.10 | |
| | | 0.2 | −0.671 | 0.83 | 0.196 | 0.098 | |
| | | 0.1 | −0.664 | 0.65 | 0.50 | 0.125 | |
| | (1.9) | 0.5 | −0.680 | 0.90 | 0.105 | 0.105 | |
| | | 0.1 | −0.666 | 0.63 | 0.55 | 0.137 | |
| $(HMB)_2Fe^0$ | (1.9) | 1.0 | −1.875 | 0.93 | 0.073 | | 0.19 |
| | | 0.5 | −1.872 | 0.89 | 0.19 | | 0.15 |
| $(DUR)_2Fe^+$ | (4.3) | 25.6 | −0.585 | 0.83 | 0.193 | 12.3 | |
| | | 12.8 | −0.583 | 0.72 | 0.344 | 11.5 | |
| | | 6.4 | −0.583 | 0.56 | 0.76 | 12.3 | |
| | | 3.2 | −0.580 | 0.35 | 2.7 | 21.6 | |
| $(DUR)_2Fe^0$ | (4.3) | 200 | −1.795 | 0.98 | 0.027 | | 11.3 |
| | | 50 | −1.794 | 0.9 | 0.105 | | 10.9 |
| | | 25 | −1.793 | 0.74 | 0.33 | | 17.2 |
| $(MES)_2Fe^+$ | (5.1) | 51.2 | −0.491 | 0.83 | 0.193 | 24.7 | |
| | | 25.6 | −0.489 | 0.7 | 0.4 | 25.6 | |
| | | 12.8 | −0.488 | 0.56 | 0.77 | 24.6 | |
| | | 6.4 | −0.481 | 0.38 | 2.5 | 40 | |
| | (1.4) | 25.6 | −0.490 | 0.68 | 0.44 | 28.2 | |
| | | 6.4 | −0.482 | 0.36 | 2.6 | 41.6 | |
| $(MES)_2Fe^0$ | (3.8) | 200 | −1.671 | 0.68 | 0.446 | | 162 |
| | | 100 | −1.668 | 0.52 | 0.878 | | 160 |

[a] In acetonitrile solution containing 0.1 *M* TBAH at 25°C, as described in the text. [b] Reversible half wave potential $E_{1/2}$ *vs.* ferrocene taken as $E_1$ ($Ar_2Fe^+$) or $E_2$ ($Ar_2Fe^0$). [c] Time to scan from $E^0$ to the switching potential. [d] Apparent rate constants for decomposition of $Ar_2Fe^+$ ($k'_1$) and $Ar_2Fe^0$ ($k'_2$) based on the EC mechanism.

By contrast, the bis(arene)iron(II) complexes with weaker arene donor ligands, *viz.*, $(DUR)_2Fe^{2+}$ and $(MES)_2Fe^{2+}$, exhibited a different electrochemical behavior at similar potential scan rates. For example, Fig. 1B shows the cyclic voltammogram of $(DUR)_2Fe^{2+}$ obtained at the scan rate of 0.5 V $s^{-1}$ in a 3.7 m*M* solution. The cathodic peak $P_1$ was roughly half that observed for $(HMB)_2Fe^{2+}$ under the same experimental conditions, and showed no return anodic wave. Most notably, it was followed by a set of new peaks. Thus instead of peak $P_2$, there was a different cathodic peak C that showed a characteristic current crossing upon the scan reversal. The unusual appearance of the anodic peak A that was coupled to the irreversible cathodic peak C was diagnostic of anodic iron stripping at a potential of *ca.* 0.3 V following its electroreductive deposition at *ca.* −1.4 V [13–15]. The latter was confirmed by the striking similarity of CV peaks C and A to those independently obtained from the ferrous ion $Fe(NCCH_3)_6^{2+}$ in Fig. 1C to reflect the cathodic deposition/anodic stripping of iron from the platinum electrode, *i.e.*:

$$Fe(NCCH_3)_6^{2+} \underset{A}{\overset{C}{\rightleftharpoons}} Fe_s + CH_3CN \qquad (6)$$

where the subscript s refers to an electrode deposit. Note that $Fe(NCCH_3)_6^{2+}$

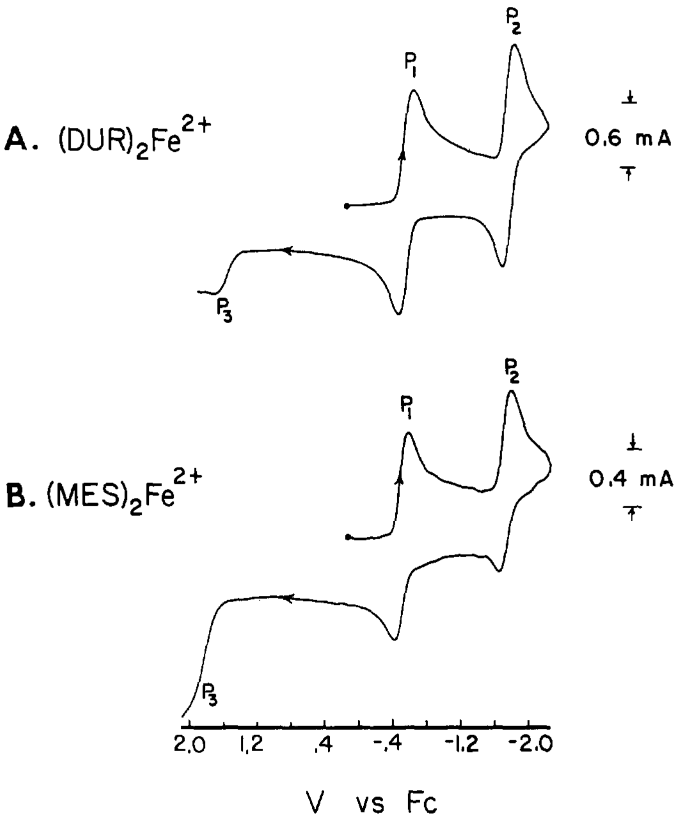

Fig. 2. Comparative cyclic voltammograms of (A) 4.3 m*M* $(DUR)_2Fe^{2+}$, and (B) 3.5 m*M* $(MES)_2Fe^{2+}$ at $v = 200$ V $s^{-1}$.

reduced in peak C can be formed by the oxidation of $Fe(NCCH_3)_6^+$ at the electrode and/or in the homogeneous electron transfer by $Ar_2Fe^{2+}$ (see Discussion). Finally, the large anodic peak $P_3$ that accompanied the chemical (reversible) change in eq. 6 was readily assigned to the oxidation of liberated durene by comparison with that of an authentic sample of the free arene ligand. We infer from the CV results in Fig. 1B and 1C that the monocation $(DUR)_2Fe^+$ formed at potentials of the peak $P_1$ was unstable on the time scale of seconds, and it decomposed with the liberation of the arene ligands, *e.g.*:

$$(DUR)_2Fe^+ \rightarrow 2DUR + Fe(NCCH_3)_6^+ \qquad (7)$$

The same conclusion applied to $(MES)_2Fe^{2+}$, but to an even more pronounced degree that was qualitatively indicated by the restoration of chemical reversibility of the redox couples only at faster scan rates in the cyclic voltammetric experiments. For example, Fig. 2 presents two nearly reversible couples $(DUR)_2Fe^{2+}/(DUR)_2Fe^+$ and $(DUR)_2Fe^+/(DUR)_2Fe^0$ on a cyclic voltammogram recorded at 200 V $s^{-1}$, with peak current ratios of $i_p^a/i_p^c = 0.86$ and 0.98 V, respectively. By comparison, the voltammogram of $(MES)_2Fe^{2+}$ at the same CV scan rate showed the significantly reduced values of $i_p^a/i_p^c = 0.68$ and 0.68, to reflect the decreased

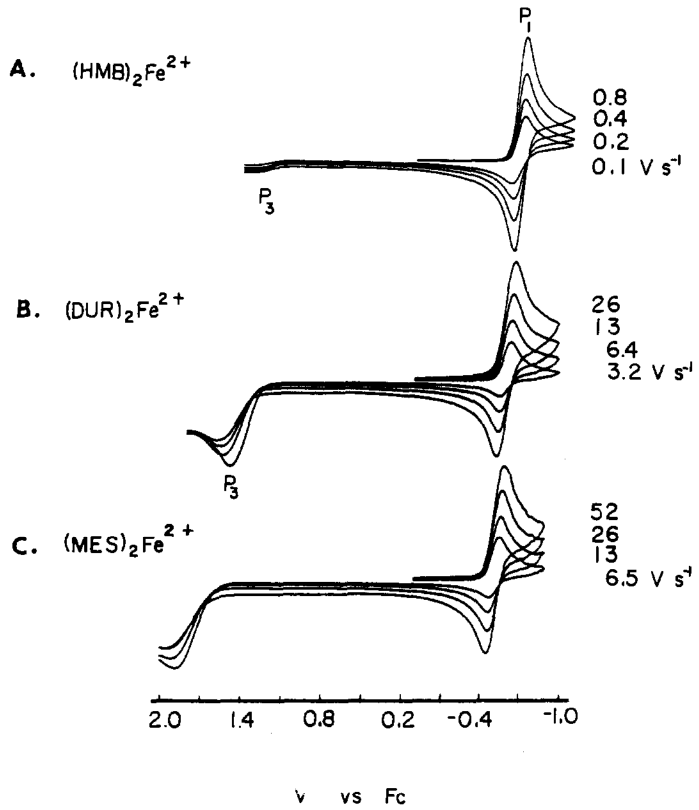

Fig. 3. Scan-rate dependence of the peak current ratio from the $Ar_2Fe^{2+/+}$ couple at $P_1$ from Ar = HMB (A), DUR (B) and MES (C) at $v$ ($V\ s^{-1}$) indicated.

stability of both $(MES)_2Fe^+$ and $(MES)_2Fe^0$. Moreover, Fig. 3 illustrates the consistently increased yields of free arene ($P_3$) that were co-produced at progressively slower scan rates, when the potential sweep was judiciously reversed just after peak $P_1$ (so that only $Ar_2Fe^+$ was electrogenerated).

Systematic studies of the scan rate dependences of the peak current ratios in Table 1 established the comparative stabilities of both $Ar_2Fe^+$ and $Ar_2Fe^0$ with the change in the arene ligand. The fitting of the peak current ratios $i_p^a/i_p^c$ for $P_1$ and $P_2$ to the working curve established by Nicholson and Shain [16] (for a simple EC formulation) led to the apparent, first-order rate constants $k_1'$ and $k_2'$ listed in Table 1 (columns 7 and 8) for $Ar_2Fe^+$ and $Ar_2Fe^0$, respectively. The limited reproducibility of the voltammograms recorded at scan rates slower than those reported in Table 1 discouraged a more extensive study of arene deligation by cyclic voltammetry. Thus the iron deposition/anodic stripping peaks were difficult to reproduce at slow scan rates, and even traces of iron deposits on the platinum electrode surface distinctly affected the electrode behavior of bis(arene)iron(II) and free arene. Since small, variable amounts of metallic iron, as revealed by its anodic stripping curve A, were also deposited on the platinum electrode during slow CV experiments even at potentials less negative than −1.1 V, a thermal disproportionation of $Fe(NCCH_3)_6^+$ is also possible.

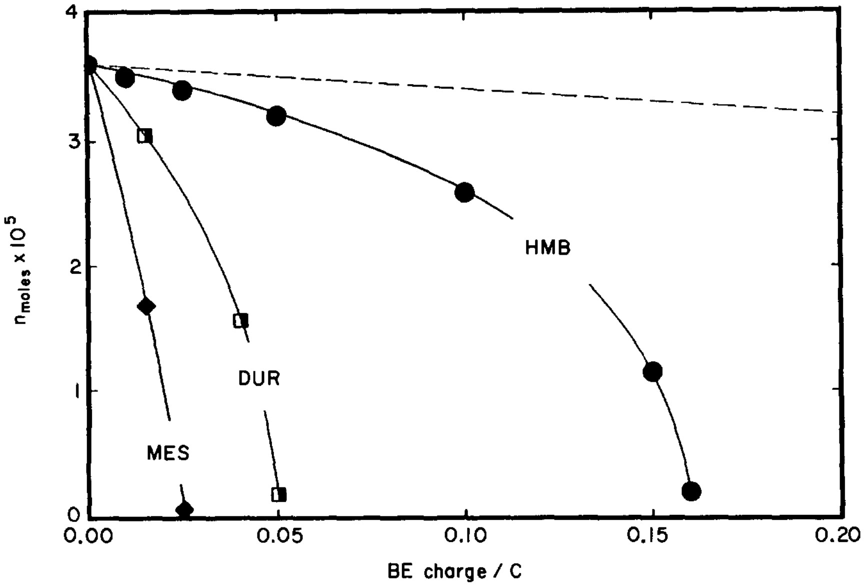

Fig. 4. Dependence of the number of moles ($n$) of $Ar_2Fe^{2+}$ remaining in solution on the charge (coulombs) passed during bulk electrolysis from Ar = MES, DUR and HMB as indicated. See text for the significance of the dashed line.

## *II. Stoichiometry and current efficiency for the reductive deligation of bis(arene)iron(II) cations*

The bulk electrolysis of the bis(arene)iron(II) salts was carried out in acetonitrile to establish the products and stoichiometry of the deligation process. During electrolysis at constant potential (*ca.* 100 mV more negative than the potential of voltammetric peak $P_1$), the concentration change of $Ar_2Fe^{2+}$ in the bulk solution was periodically monitored with the aid of normal pulse voltammetry (see below) [17,18]. Typical variations in the number of moles of $Ar_2Fe^{2+}$ in the course of the electrolysis are illustrated in Fig. 4. For each bis(arene)iron(II) dication, the characteristic coulometric behavior, showing an apparent acceleration of the electrolysis at longer times, revealed an unexpected catalytic contribution to the overall process. Importantly, the total charge required to achieve the full chemical transformation varied, but it was always significantly less than one faraday per mole of $Ar_2Fe^{2+}$, the apparent catalytic turnover number (CTN) being 20 for $(HMB)_2Fe^{2+}$, 75 for $(DUR)_2Fe^{2+}$ and 150 for $(MES)_2Fe^{2+}$ at 25°C.

The products of the bulk electrolysis were quantitatively assayed by normal pulse voltammetry (NPV) owing to the disturbance of the cyclic voltammograms caused by the electrodeposition of metallic iron (*vide supra*). Normal pulse voltammetry, on the other hand, minimizes the deleterious effects of product precipitation [19,20], and the limiting current is simply proportional to the number of electrons involved in the electrolysis. As a result, the concentration of an analyte can be measured directly [17]. For example, the NP voltammogram 1 in Fig. 3 shows the one-electron cathodic wave ($P_1$) of 3.0 m*M* $(HMB)_2Fe^{2+}$ in the solution before electrolysis at the half wave potential of *ca.* −0.5 V. Likewise, the products of electrolysis were observed as a pair of cathodic and anodic waves in the normal

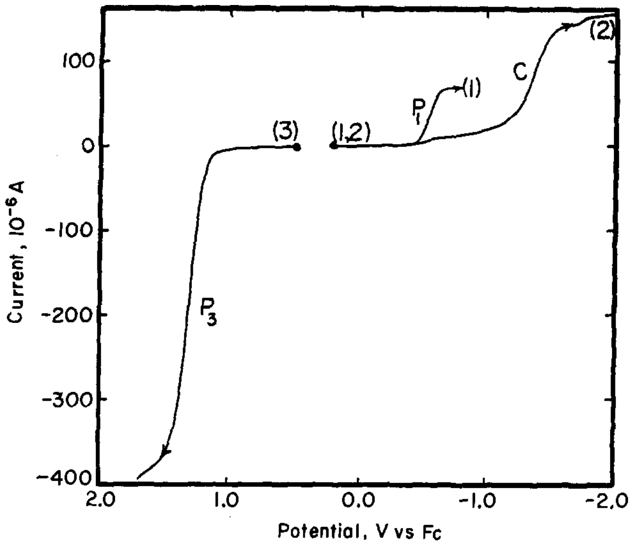

Fig. 5. Normal pulse (NP) voltammogram from 3.0 m*M* $(HMB)_2Fe^{2+}$ in acetonitrile (1) before and (2, 3) after bulk electrolysis, where half-wave potentials for $P_1$, C and $P_3$ retain their significance from the cyclic voltammogram in Fig. 1B.

pulse voltammograms. Thus, the NP voltammogram 2 (Fig. 5) shows a large cathodic wave (*C*) at *ca.* −1.5 V which is almost twice as large as the initial wave $P_1$; and the NP voltammogram 3 shows an anodic wave ($P_3$) at 1.2 V which is roughly five times larger than $P_1$. The half wave potential of the NPV wave $P_3$ coincided with that obtained from an authentic sample of hexamethylbenzene, and the limiting current of this wave corresponded to the concentration of 6.2 mM HMB. The assignment of the NPV wave $P_2$ was similarly based on its comparison with the 2-electron reduction of $Fe(NCCH_3)_6^{2+}$ in acetonitrile, and the concentration of 3.05 m*M* iron(II) was evaluated from the limiting current at −1.7 V. This electrochemical measurement was confirmed by complexation of $Fe(NCCH_3)_6^{2+}$ with 2,2′-bipyridine followed by the spectrophotometric determination of $Fe(bpy)_3^{2+}$ quantitatively. The measurement at $\lambda$ 520 nm with $\epsilon = 8560\ M^{-1}\ cm^{-1}$ indicated a concentration of 3.0 m*M* $Fe(bpy)_3^{2+}$ in aqueous acetonitrile [21]. The results of the bulk electrolysis (E) of the bis(arene)iron(II) dications thus establish the overall stoichiometry to be

$$Ar_2Fe^{2+} \xrightarrow{[E]} 2Ar + Fe(NCCH_3)_6^{2+} \tag{8}$$

within the experimental restrictions of the high catalytic turnover numbers obtained for $(HMB)_2Fe^{2+}$, $(DUR)_2Fe^{2+}$, and $(MES)_2Fe^{2+}$ (see above).

## Discussion

The reversible potentials for the reduction of bis(arene)iron(II) dications to $Ar_2Fe^+$ and the subsequent reduction of the monocation to $Ar_2Fe^0$, as given by $E_1^\circ$ and $E_2^\circ$, respectively, in Table 1 are both linearly related to the reversible oxidation potential of the (uncomplexed) arene ligand of $E_{Ar}^\circ$ = 1.25, 1.43 and 1.66

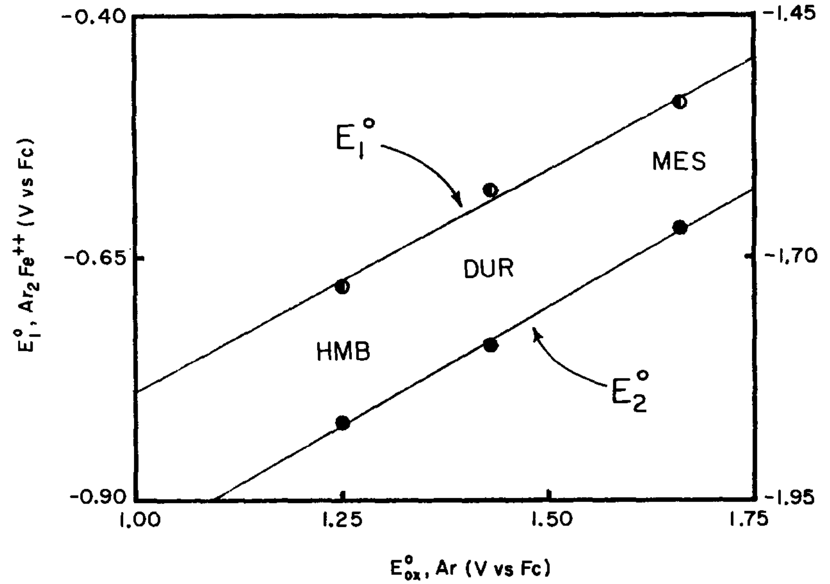

Fig. 6. Correlation of the reduction potentials $E^\circ_1$ and $E^\circ_2$ for $Ar_2Fe^{2+}$ and $Ar_2Fe^{+}$, respectively, with the oxidation potential $E^\circ_{Ar}$ of the uncomplexed arene ligand in acetonitrile.

V *vs.* ferrocene for Ar = hexamethylbenzene (HMB), durene (DUR), and mesitylene (MES), respectively [22]. The linear relationships shown in Fig. 6 in acetonitrile solution are expressed in volts as:

$$E^\circ_1(Ar_2Fe^{2+/+}) = 0.46E^\circ_{Ar} - 1.3 \qquad (9)$$

$$E^\circ_2(Ar_2Fe^{+/0}) = 0.49E^\circ_{Ar} - 2.5 \qquad (10)$$

Thus, eqs. 9 and 10 show that the acceptor properties of both $Ar_2Fe^{2+}$ and $Ar_2Fe^{+}$ respond to the ligand donicity in essentially the same way, despite a difference of almost 30 kcal mol$^{-1}$ between $E^\circ_1$ and $E^\circ_2$.

The cyclic voltammetric examination of bis(arene)iron(II) dications reveals a striking difference in the temporal persistence of each of these species in acetonitrile solution, as graphically underscored in Fig. 1 (Table 1). Cyclic voltammetry also shows (Figs. 2 and 3) the instability of bis(arene)iron(II) dications under reducing conditions to arise from the transient character of the monocation, the lifetime of $Ar_2Fe^{+}$ decreasing monotonically from roughly $\tau = 10$ s to as short as 80 and 40 ms from Ar = HMB, DUR and MES, respectively. Since this trend parallels the variation in the donor strength of the arene ligand, the deligation process can be ascribed to the spontaneous decomposition of the monocation according to the stoichiometry:

$$Ar_2Fe^{+} \xrightarrow{CH_3CN} 2Ar + Fe(NCCH_3)_6^{+} \qquad (11)$$

Indeed such a spontaneous decomposition is consistent with the charge-transfer formulation in Scheme 1, since the subsequent oxidation of $Fe(NCCH_3)_6^{+}$ by the donor cation ($D^{+}$) leads to the overall stoichiometry in eq. 2. By analogous reasoning, the catalytic turnover numbers for the electroreductive deligation of

$Ar_2Fe^{2+}$ of CTN = 20, 75 and 150 for Ar = HMB, DUR and MES, respectively, as revealed in the bulk electrolysis study (Fig. 4), indicate that $Fe(NCCH_3)_6^+$ is rapidly oxidized at the electrode potential ($P_1$) of the first CV wave. If so, the electrocatalysis for arene deligation can be represented as the ECE mechanism.

$$Ar_2Fe^{2+} + e \xrightarrow{[P_1]} Ar_2Fe^+ \qquad (12)$$

$$Ar_2Fe^+ \xrightarrow[CH_3CN]{k_1} 2Ar + Fe(NCCH_3)_6^+ \qquad (13)$$

$$Fe(NCCH_3)_6^+ \xrightarrow{[P_1]} Fe(NCCH_3)_6^{2+} + e \qquad (14)$$

Scheme 2.

It must be emphasized, however, that if $Fe(NCCH_3)_6^+$ is rapidly oxidized at the electrode potential $P_1$, it will also be capable of fast electron transfer to the bis(arene)iron dication itself, particularly in view of the electrochemical reversibility of the $Ar_2Fe^{2+/+}$ couple at $P_1$ (see above) to accord with the low intrinsic barrier (reorganization energy) for the reduction of the bis(arene)iron dication [23]. Thus electrocatalysis of arene deligation by the alternative homogeneous oxidation of $Fe(NCCH_3)_6^+$ can be represented as the HOMO mechanism in Scheme 3.

$$Ar_2Fe^{2+} + e \xrightarrow{[P_1]} Ar_2Fe^+ \qquad (15)$$

$$Ar_2Fe^+ \xrightarrow[CH_3CN]{k_1} 2Ar + Fe(NCCH_3)_6^+ \qquad (16)$$

$$Fe(NCCH_3)_6^+ + Ar_2Fe^{2+} \overset{K_1}{\rightleftharpoons} Fe(NCCH_3)_6^{2+} + Ar_2Fe^+, \textit{etc.} \qquad (17)$$

Scheme 3.

The electrocatalytic mechanisms in Schemes 2 and 3 differ basically by whether $Fe(NCCH_3)_6^+$ undergoes a heterogeneous or homogeneous oxidation [24,25]. In both cases, the number of electrons consumed for each $Ar_2Fe^{2+}$ deligated would tend to decrease to the limiting value of zero, the catalytic inefficiency being $(CTN)^{-1}$. Insofar as the electrochemical deligation of $Ar_2Fe^{2+}$ is concerned, the extent to which the homogeneous oxidation of $Fe(NCCH_3)_6^+$ dominates over the heterogeneous (electrode) oxidation would lead to a catalytic process which extends further into the bulk of the solution [25]. As such, transient electrochemical methods should provide the means to examine the contribution from each pathway. Toward this end, the experimental peak current ratios obtained at various scan rates were compared with the working curves evaluated from the computer-simulated cyclic voltammograms in Fig. 7 (see the Experimental section for details). The first-order rate constants $k_1$ for the decomposition of $Ar_2Fe^+$ are evaluated in Table 2 for the ECE and HOMO mechanisms. Clearly, the values of $k_1$ (ECE) and $k_1$ (HOMO) as listed in columns 4 and 5, respectively, are insufficiently differentiated to draw any mechanistic conclusion. Within the accuracy of the CV peak current ratios [26], and the range of scan rates that were limited by experimental difficulties at the slower timescales (see above), similar results were obtained for the ECE and HOMO mechanisms. Indeed, previous workers have generally found that the differences between cyclic voltammograms

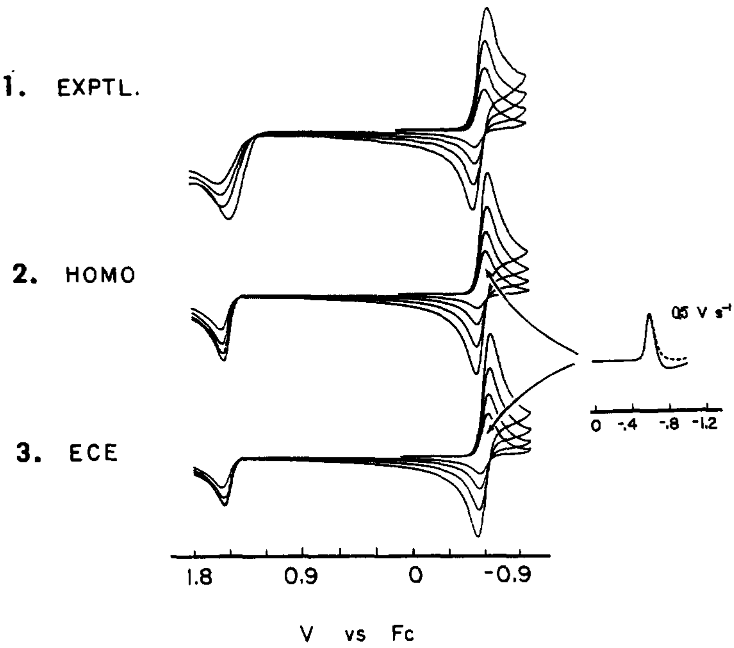

Fig. 7. Experimental (1) and simulated (2) HOMO and (3) ECE cyclic voltammograms for the first wave $P_1$ of 4.3 m*M* $(DUR)_2Fe^{2+}$ in Fig. 3B. The inset shows the simulated linear-sweep voltammogram on the negative scan at the slow rate of $v = 0.5$ V $s^{-1}$ from HOMO (———) and ECE (— — —) mechanisms.

for alternative mechanisms with and without homogeneous electrontransfer steps to be rather subtle [27]. For example, one qualitative feature of the simulated cyclic voltammograms, also noted by Feldberg and Jeftic [28], identifies the

Table 2

Rate constants for the first-order deligation of $Ar_2Fe^+$ based on the ECE and HOMO mechanisms [a]

| Ar | $v$ (V $s^{-1}$) | $\frac{i_p^a}{i_p^c}$ | $k_1$ (ECE) [b] ($s^{-1}$) | $k_1$ (HOMO) [c] ($s^{-1}$) |
|---|---|---|---|---|
| HMB | 1.6 | 0.98 | 0.107 | 0.107 |
| | 0.8 | 0.96 | 0.10 | 0.10 |
| | 0.4 | 0.91 | 0.10 | 0.10 |
| | 0.2 | 0.83 | 0.098 | 0.098 |
| | 0.1 | 0.65 | 0.125 | 0.117 |
| DUR | 25.6 | 0.83 | 12.3 | 12.3 |
| | 12.8 | 0.72 | 11.5 | 11.5 |
| | 6.4 | 0.56 | 11.5 | 10.1 |
| | 3.2 | 0.35 | 12.8 | 9.3 |
| MES | 51.2 | 0.83 | 24.7 | 24.7 |
| | 25.6 | 0.7 | 25.6 | 25.6 |
| | 12.8 | 0.56 | 22.8 | 20.1 |
| | 6.4 | 0.36 | 25.2 | 18.2 |

[a] Peak current ratios for CV peak $P_1$ from Table 1. [b] By CV simulation based on Scheme 2. [c] From Scheme 3.

Table 3

First-order rate constants for the deligation of $Ar_2Fe^0$ by CV simulation of the peak current ratios

| Ar | $v$ (V $s^{-1}$) | $k_2$ ($s^{-1}$) | $i_p^a/i_p^c$ ($P_1$) | | $i_p^a/i_p^c$ ($P_2$) | |
|---|---|---|---|---|---|---|
| | | | Exp. | Calc. | Exp. | Calc. |
| HMB | 1.0 | 0.02 | 0.91 | 0.91 | 0.98 | 0.99 |
| | 0.5 | 0.02 | 0.85 | 0.85 | 0.90 | 0.89 |
| DUR | 200 | 20 | 0.88 | 0.89 | 0.98 | 0.99 |
| | 50 | 20 | 0.68 | 0.68 | 0.90 | 0.89 |
| MES | 200 | 250 | 0.68 | 0.68 | 0.68 | 0.68 |
| | 100 | 250 | 0.53 | 0.53 | 0.52 | 0.51 |

Experimental peak current ratios for CV peaks $P_1$ and $P_2$ from Table 1. Calculated peak current ratios as described in the text.

contribution from the homogeneous electron transfer (eq. 17) that can lead to a decay of the post-peak current to below the zero line (see Fig. 7, inset). Experimentally, this small effect is often obscured by the charging current in the CV experiments. Unfortunately, the erratic behavior of $Ar_2Fe^{2+}$ in slow CV experiments precluded our detailed examination of this potential range.

In order to quantitatively evaluate the lability of the uncharged species $Ar_2Fe^0$ to deligation, *e.g.*:

$$Ar_2Fe^0 \xrightarrow[CH_3CN]{k_2} 2Ar + Fe(NCCH_3)_6^0, \textit{ etc.} \tag{18}$$

the fast scan cyclic voltammograms similar to those shown in Fig. 2 were simulated with the aid of the electrochemical and kinetics parameters used in the simulation of Scheme 3 (4) together with that for the decomposition of $Ar_2Fe^0$ in eq. 18. Furthermore, the large difference in $E_1^\circ$ and $E_2^\circ$ necessitated the inclusion of the fast comproportionation reaction, *i.e.*

$$Ar_2Fe^0 + Ar_2Fe^{2+} \overset{K_2}{\rightleftharpoons} 2Ar_2Fe^+ \tag{19}$$

which is expected to be diffusion controlled ($> 10^{10}$ $M^{-1}$ $s^{-1}$) from the Marcus treatment [29]. The results of fitting the experimental peak current ratios to the working curves constructed from peak current ratios in the simulated cyclic voltammograms (see Experimental section) are listed in Table 3. Most notably the lifetimes of the uncharged species: $(HMB)_2Fe^0$, $(DUR)_2Fe^0$, and $(MES)_2Fe^0$ are found to decrease in the same qualitative order (*i.e.*, $\tau = 50$, 0.05, and 0.004 s) as the corresponding series of monocations included in Table 2.

Transient and steady-state electrochemical analyses thus indicate the applicability of the EC mechanism for arene deligation during the electrochemical reduction of bis(arene)iron(II) dications, and identify the monocation $Ar_2Fe^+$ as the reactive intermediate. However the follow-up process involving the oxidation of $Fe(NCCH_3)_6{}^+$ either (a) heterogeneously at the electrode or (b) by homogeneous electron transfer with $Ar_2Fe^{2+}$ cannot be differentiated by cyclic voltammetric analysis. Since this dichotomy is commonly encountered [27], we hope that pulse techniques (which minimize the voltammetric complication from iron deposition and discriminate against charging currents) will resolve this important mechanistic question in electrocatalysis.

## Experimental

### *Materials*

The crystalline bis(arene)iron(II) hexafluorophosphate salts were prepared by the treatment of mesitylene or durene with anhydrous ferric chloride (Pennwalt) and aluminum chloride (Fluka) according to the literature procedure [30,31]. The hexamethylbenzene derivative $(HMB)_2Fe^{2+}(PF_6^-)_2$ was prepared from ferrous chloride, aluminum chloride and hexamethylbenzene by an analogous procedure [32]. Tetra-n-butylammonium hexafluorophosphate (Johnson Matthey) was recrystallized from acetonitrile and dried *in vacuo*. Acetonitrile (HPLC grade, Fisher) was stirred for 24 h with $KMnO_4$ (0.1% by weight), then heated to boiling, cooled and filtered from the brown $MnO_2$ residue. The filtered acetonitrile was distilled from $P_2O_5$ (2 g $L^{-1}$) and redistilled from $CaH_2$ under an atmosphere of argon.

### *Instrumentation*

All voltammetric experiments were performed with a BAS 100B electrochemical analyzer using the conventional three-electrode arrangement. A platinum disk electrode (BAS) served as the working electrode and was referenced to $Ag^+/Ag$ (0.01 M AgCl*O*4 and 0.1 *M* $TBAPF_6$ in acetonitrile) or an aqueous SCE reference electrode. Both reference electrodes were calibrated with a ferrocene standard [9] and all potentials in this work are referred to the potential of $Cp_2Fe$. A platinum flag electrode was used as the auxiliary electrode. Bulk electrolyses were performed on a PAR Model 173 potentiostat equipped with a PAR Model 179 coulometer.

### *Bulk electrolysis of bis(arene)iron(II) salts*

In a typical bulk electrolysis experiment, 12 mL of a 3.0 m*M* acetonitrile solution of the bis(arene)iron(II) salt was electrolyzed at a constant potential of the Pt flag electrode, which was kept at either 0.1 V (HMB) or 0.2 V (DUR, MES) more negative value than the $E_{1/2}$ value determined from CV experiments. Changes of the bulk concentration of $Ar_2Fe^{2+}$ during the course of electrolysis were monitored by normal pulse voltammetry during which the electrolysis was interrupted momentarily. The results illustrated in Fig. 4 show the simple electrolysis of 36 $\mu$mol of $Ar_2Fe^{2+}$, for which the total charge of 3.47 $C_{ex}$ would have been consumed on the basis of a 1 : 1 electrochemical stoichiometry. The dashed line in Fig. 4 thus represents the expected dependence of $Ar_2Fe^{2+}$ concentration on the electrolysis charge. The catalytic turnover numbers were calculated as CTN = $3.47/C_{ex}$.

### *Cyclic and normal pulse voltammetry of bis(arene)iron(II) dications*

Owing to the photosensitivity of bis(arene)iron(II) salts, the solutions of the salts in acetonitrile were very carefully protected from light. Special precautions were always taken to avoid contamination by moisture. The electrochemical cell was of air-tight design with high-vacuum teflon valves and viton O-ring seals to allow an inert atmosphere to be maintained without contamination by grease [33]. The reference electrode was separated from the solution by a cracked glass tip. The cyclic voltammograms measured at slow scan rates were especially difficult to reproduce, since variable amounts of metallic iron (revealed by its diagnostic anodic stripping currents shown in Fig. 1C) were deposited on the platinum surface. Since this deposition occurred even when the negative scan CV was limited to the narrow potential scan shown in Fig. 3, disproportionation of 2 $Fe(NCCH_3)_6^+ \rightarrow Fe_s + Fe(NCCH_3)_6^{2+}$ is inferred. However, it is noteworthy that the limiting current in normal pulse voltammetry was unaffected by the metallic iron deposit on the platinum electrode, and the concentration of $Fe(NCCH_3)_6^{2+}$ determined from the NPV wave agreed well with that measured with $Fe(bpy)_3^{2+}$ spectrophotometrically. In utilizing Nicholson and Shain's working curves (which are limited to current ratio greater than 0.4) [16], they were extended to the lower values of $i_p^a/i_p^c = 0.3$ obtained from the simulated cyclic voltammograms (see below) for use in Table 1.

### *Computer simulation of the cyclic voltammograms*

The computer simulation of the experimental cyclic voltammograms was carried out with the aid of Gosser's PASCAL program based on Feldberg's algorithms [34,35]. The following set of electrochemical parameters was employed: $E_1^\circ = 0.60$ and $-1.08$ V, $k_s = 0.05$ and $0.15$ cm $s^{-1}$, and $\alpha = 0.5$ for the redox couples in eqs. 12 and 14, respectively. Note the magnitude of $E^\circ$ for $Fe(NCCH_3)_6^+$ was the least negative value, based on the absence of its anodic peak in either Fig. 3 or 7. The working curves of $i_p^a/i_p^c$ *versus* the apparent rate constant ($k\tau$) for the ECE mechanism in Scheme 2 were constructed from the results in Table 2. Typical cyclic voltammograms such as that presented in Fig. 3 were simulated with these parameters and the value of $k_1$ (ECE) in Table 2. For a similar working curve for the HOMO mechanism in Scheme 3, the homogeneous electron transfer rate constant $k_f$ was set as $1 \times 10^5$ $M^{-1}$ $s^{-1}$ and the microscopic reverse $k_b$ was 0.01 $M^{-1}$ $s^{-1}$ to correspond to $K_1$ calculated from the potential difference $E_1^\circ - E^\circ$. The calculated peak current ratio showed no dependence on $k_f > 10^4$ $M^{-1}$ $s^{-1}$. Typical cyclic voltammograms such as that shown in Fig. 2 were simulated with these parameters and the value of $k_1$ (HOMO) in Table 2.

The deligation of the neutral species $Ar_2Fe^0$ was based on the electrochemical and kinetic parameters given above in the addition to $E_2^\circ$ in Table 1 and the comproportionation equilibrium constant $K_2$ calculated from the values of $E_1^\circ$ and $E_2^\circ$. In the range of fast scan rates used in these experiments, the difference between the ECE and HOMO mechanisms at $P_1$ was negligible (see the inset to Fig. 7). Thus only $k_2$ was optimized, and the values obtained are listed in Table 3.

## Acknowledgments

We thank D.K. Gosser, Jr. for kindly providing us with a copy of his CV Sim Program, the National Science Foundation, R.A. Welch Foundation and the Texas Advanced Research Program for financial support. Z.J.K. thanks the University of Warsaw for leave of absence.

## References

1 (a) E.O. Fischer and R. Böttcher, Chem. Ber., 89 (1956) 2937; (b) E.O. Fischer and J. Müller, *ibid.*, 96 (1963) 3217; *idem*, Z. Naturforsch., Teil B, 17 (1962) 776.

2 T.S. Cameron, M.D. Clerk, A. Linden, K.C. Sturge and M.J. Zaworotko, Organometallics, 7 (1988) 2571.

3 D. Astruc, Acc. Chem. Res., 19 (1986) 377. D. Mandon and D. Astruc, Organometallics, 9 (1990) 341 and Synlett, (1991) 369 and references therein.
4 R.E. Lehmann and J.K. Kochi, J. Am. Chem. Soc., 113 (1991) 501.
5 D.M. Braitsch, J. Chem. Soc., Chem. Commun., (1974) 460.
6 R.S. Mulliken, J. Am. Chem. Soc., 74 (1952) 811.
7 R.S. Mulliken and W.B. Person, Molecular Complexes, Wiley, New York, 1969.
8 E.O. Fischer and F. Rohrscheid, Z. Naturforsch., Teil B, 17 (1962) 483.
9 (a) R.R. Gagne, C.A. Koval and G.C. Lisensky, Inorg. Chem., 19 (1980) 2854; (b) G. Gritzner and J. Kuta, Pure Appl. Chem., 56 (1984) 461.
10 See also: (a) M.I. Montenegro and D. Pletcher, J. Electroanal. Chem., 200 (1986) 371; (b) D.O. Wipf, E.W. Kristensen, M.R. Deakin and R.M. Wightman, Anal. Chem., 60 (1988) 306; (c) A.M. Bond, T.L.E. Henderson, T.F. Mann, W. Thormann and C.G. Zoski, *ibid.*, 60 (1988) 1878.
11 Z. Galus, Fundamentals of Electrochemical Analysis, Ellis Harwood, Chichester, 1976.
12 J.O. Howell, J.M. Goncalves, C. Amatore, L. Klansic, R.M. Wightmann and J.K. Kochi, J. Am. Chem. Soc., 106 (1984) 3968.
13 Kh.Z. Brainina, Stripping Voltammetry in Chemical Analysis, Wiley, New York, 1974.
14 T. Brezins and P. Delahay, J. Am. Chem. Soc., 75 (1953) 555.
15 G.J. Hills, D.J. Schiffrin and J. Thompson, Electrochim. Acta, 19 (1974) 657.
16 R.S. Nicholson and I. Shain, Anal. Chem., 36 (1964) 706.
17 G.C. Barker and A.W. Gardner, Z. Anal. Chem., 173 (1960) 79.
18 E.P. Parry and R.A. Osteryoung, Anal. Chem., 37 (1965) 1634.
19 W. O'Deen and R.A. Osteryoung, Anal. Chem., 43 (1971) 1871.
20 Z.J. Karpinski, in A. Iwaska (Ed.), ElectroFinnAnalysis, Plenum, New York, 1991.
21 D.H. Busch and J.C. Bailar, Jr., J. Am. Chem. Soc., 78 (1956) 1137.
22 C. Amatore and J.K. Kochi, Adv. Electron-Transfer Chem., 1 (1991) 55.
23 M.J. Weaver, in R.G. Compton (Ed.), Comprehensive Chemical Kinetics, Vol. 27, Elsevier, Amsterdam, 1987, Chapter 1.
24 M.D. Hawley and S.W. Feldberg, J. Phys. Chem., 70 (1966) 3459.
25 S.W. Feldberg, J. Phys. Chem., 75 (1971) 2377.
26 Compare: A.J. Bard and L.R. Faulkner, Electrochemical Methods, Wiley, New York, 1980, p. 229 and ref. 8.
27 D.H. Evans, Chem. Rev., 90 (1990) 739 and references therein.
28 (a) L. Jeftic and S.W. Feldberg, J. Phys. Chem., 75 (1971) 2381; (b) S.W. Feldberg and L. Jeftic, J. Phys. Chem., 76 (1972) 2439.
29 R.A. Marcus, J. Phys. Chem., 67 (1963) 853.
30 J.F. Helling and D.M. Braitsch, J. Am. Chem. Soc., 92 (1970) 7207.
31 J.F. Helling, S.L. Rice, D.M. Braitsch and T. Mayer, J. Chem. Soc., Chem. Commun., (1971) 930.
32 D. Mandon and D. Astruc, J. Organomet. Chem., 369 (1989) 383.
33 D.J. Kuchynka, C. Amatore and J.K. Kochi, Inorg. Chem., 25 (1986) 4087.
34 D.K. Gosser and P.H. Rieger, Anal. Chem., 60 (1988) 1159.
35 S.W. Feldberg, Electroanal. Chem., 3 (1969) 199; *idem*, in H.B. Mark (Ed.), Computer Applications in Analytical Chemistry, Dekker, New York, 1972, p. 185 ff.